JOURNAL OF APPLIED ELECTROCHEMISTRY 18 (1988) 62–74

Applicability of four recent models to the discharge behaviour of different phases of MnO_2 in alkaline and acidic/neutral electrolytes

BUQUI D. DESAI*, R. A. S. DHUME, V. N. KAMAT DALAL

Department of Chemistry, Goa University, Bambolim, P.O. Santa Cruz, Goa – 403 005, India

Received 18 February 1987; revised 27 June 1987

Manganese dioxides belonging to different crystalline phases were discharged in 9 M KOH and 5 M NH_4Cl + 2 M $ZnCl_2$ at a constant current of 1 mA 0.1 g. These phases were characterized by X-ray diffractometry and chemical analysis. Four different models were tried for their applicability to the discharge behaviour of these phases. Almost all the four models successfully predict the values of the oxyhydroxides in the first half of the reduction range $0 < r < 0.5$, but fail to do so in the second half i.e. $0.5 < r < 1$. The only exception to this is the model (Model 2) of Maskell, Shaw and Tye. This model yields, by far, the best match with the experimental data in acidic/neutral electrolyte. In alkaline electrolyte, however, even this model fails to account satisfactorily for the observed potentials in the lower half of the reduction. This failure could perhaps be explained as due to the formation of a new phase at about $MnO_{1.6}$ ($r \simeq 0.8$). The cation vacancy model of Ruetschi predicts most of the physical properties rather well but the match of the theoretical potentials with the experimental values is poor, specially in the lower half.

1. Introduction

The present investigation was undertaken with a view to evaluating critically some of the theoretical models proposed recently [1–4] to account for the observed variations in the open circuit voltage of the $(MnO_2)_{1-r}(MnOOH)_r$ system.

Coleman [5] was probably the first to attempt a comprehensive theoretical model for the observed potential changes during the electrochemical reduction of MnO_2. Later Johnson and Vosburgh [6] realized the importance of oxyhydroxide as the primary reduction product and proposed the following empirical formula

$$E = E^0 + 0.073 \log \frac{[MnO_2]}{[Mn_2O_3]} \quad (1)$$

Scott [7] followed by Kornfeil [8] proposed that the rate determining process in the cathodic reduction was the diffusion of protons in the γ-MnO_2 lattice. Neumann and Roda [9] suggested the following formalism for the reduction of γ-MnO_2.

$$MnO_2 + H^+ + e \rightleftharpoons MnOOH \quad (2)$$

They proposed the following expression for the potential:

$$E = E^0 + \frac{RT}{F} \ln \frac{(1 - r)\phi_{MnO_2}}{r\phi_{MnOOH}} \quad (3)$$

Kozawa and Powers [10, 11], replaced the activity term in the equation by mole fractions i.e. X_{MnO_2} and X_{MnOOH}. The curves thus obtained, however, showed insufficient rate of fall of potential compared with the observed values [12, 13].

It was Tye [14] who obtained a better representation by using ionic mole fractions. Subsequently Tye and co-workers [2, 3] developed a statistical basis for the thermodynamics of the solid solutions γ-MnO_2/δ-MnOOH. The spatial correlation coefficient which they had introduced earlier [15] was put on a firm footing. They also found thermodynamic and other evidence for the presence of two solid solutions on either side of mid-reduction point [16].

Atlung and Jacobsen [1] also used a similar approach in which the inserted protons and electrons are not assigned to discrete chemical compounds. Instead their statistical distribution on the available sites (for protons) or bands (for electrons) in the lattice was considered to be the basis of an analytical expression for the potential,

$$E = E^0 + \frac{RT}{F} \ln \frac{1 - r}{r} - \frac{\mu e}{F} \quad (4)$$

This model was, however, meant for the discharge behaviour in a strong alkaline medium.

The latest model of Tye [3] introduces yet another adjustable parameter, y, in order to obtain the best match with the experimental data.

All the above models, however, have one common feature, i.e. they are concerned with the discharge behaviour only. They do not take into account other physical properties. To that extent one could say that these models have a limited applicability, In fact, it is

* To whom all correspondence should be addressed.

0021-891X/88 $03.00 + .12

Table 1. Chemical analyses of the samples used in this work

Sample	% MnO_2	% Mn	x in MnO_{1+x}	% *Combined* H_2O 'y'	*Tap density 200 taps* $g\,cm^{-3}$
IC8	90.2	61.77	0.9229	2.423	1.667
CMD-1	91.33	60.36	0.9563	2.928	1.470
CMD-2	90.93	60.02	0.9576	2.939	1.515
ϱ	87.19	56.86	0.9691	4.424	1.478
δ	83.67	57.68	0.9167	3.105	1.250
IC4	88.75	59.88	0.9367	2.883	2.272
EMD	88.38	59.61	0.9370	3.880	2.000
AMD	82.41	55.68	0.9354	2.869	1.390

Ruetschi's [4] model which incorporates not only the discharge behaviour but also relevant physical properties such as density, structural/combined water, proton transfer rate and electronic conductivity. It, therefore, appears to be the only model known so far, which could have larger scope and therefore, a greater degree of applicability. It is, therefore, prima facie, a holistic model. In view of the foregoing discussion of the above models, it was felt that their applicability [1–4] had to be rigorously tested and critically evaluated in the light of the work carried out in this laboratory.

2. Experimental details

2.1. *Methods of preparation*

(i) Chemical manganese dioxide. The procedure of Fernandes *et al.* [17] was slightly modified to obtain a product of higher density. The $NaClO_3$ was added in small portions over a period of 1 h. The sample is labelled as CMD-2.

(ii) ϱ-MnO_2 [18]. 89.5 g of commercial MnO_2 were slowly added with constant stirring to 1.4 l of concentrated HCl and cooled to 8° C. The unreacted MnO_2 was filtered off and the filtrate was poured into 12.5 l of distilled water and the resulting product was filtered, washed, and then digested in 40% HNO_3 at 45° C for 5 h. The method for ϱ-MnO_2 preparation was taken from McKenzie [18] but the sample obtained was with a low % of available oxygen (% MnO_2) therefore, the residue was digested at 45° C with 40% HNO_3 for 5 h. The residue was filtered, washed and dried around 60° C for five days. The sample is labelled as ϱ-MnO_2.

(iii) Synthetic birnessite or δ-MnO_2 [19]. 150 g of NaBr were dissolved in 3 l of distilled water containing 30 ml of acetic acid. The solution was heated to boiling. To this hot solution 300 ml of 2% $KMnO_4$ was slowly added with constant stirring. The precipitate was boiled for 5 min and kept for 24 h at room temperature. The residue was digested in 0.5 N HNO_3 for 20 h at 40° C. The product was filtered, washed, dried and preserved. The sample is labelled as synthetic birnessite.

(iv) Electrolytic manganese dioxide (EMD) with Pb electrodes [20]. 500 ml of 0.5 M $MnSO_4 \cdot 4H_2O$ in 0.5 M H_2SO_4 was heated to maintain a temperature of 95° C. It was electrolysed using lead electrodes by passing a direct current of 1 A dm^2 for 3 h. The deposited MnO_2 on anode was detached from the surface, washed, dried and stored as earlier. The sample is labelled as EMD.

2.2. *Determination of combined water*

About 1 g of the sample was accurately weighed in a silica crucible and heated at 110° C for 1 h, cooled in a desiccator and then weighed. This dried sample was further heated for 2 h at 300° C in a furnace. It was next cooled in a desiccator and weighed again. From the loss in weight at 300° C the percentage of combined water was calculated.

2.3. *Density determination*

(i) Pycnometric density and tap density were determined by employing methods given in [21] and [22].

(ii) XRD density [4] was calculated by using the relation

$$D = \text{molecular weight}/V_0$$

where,

$$V_0 = \frac{v \times 6.02 \times 10^{23}}{z}$$

The densities so calculated are presented in Table 2.

All the samples were duly characterized by chemical analyses (Table 1), X-ray diffractography and infrared spectroscopy [23]. The lattice parameters, crystallographic density and pycnometric densities are presented in Table 2. IC4 and IC8 were used as the reference samples.

2.4. *The discharge characteristics*

(i) The discharge characteristics of the samples were investigated using two different electrolytes: 9 M KOH and 5 M NH_4Cl + 2 M $ZnCl_2$. The cell assembly used was similar to that employed by Fernandes *et al.* [24]. In the case of 9 M KOH, the cathode mix was 0.1 g of MnO_2 sample and 1 g of graphite (IC1) wetted with 0.5 ml of 9 M KOH. In the latter case the cathode mix was as follows: 0.1 g of MnO_2 with 0.5 g of acetyl-

Table 2. Lattice parameters, XRD and pycnometric densities of the different MnO_2 polymorphs

Sample	*Crystal phase*	*Lattice parameters* (nm)			*Cell volume* $(nm)^3$	*XRD density* $g\,cm^{-3}$			*Pycnometric density* $g\,cm^{-3}$‡
		a	*b*	*c*		A*	B†		
							y = 0	*y* > 0	
IC8	γ	0.4434	0.8524	0.2934	0.1109	5.2985	5.0890	4.9996	4.6668
CMD-1	γ	0.4413	0.8783	0.2894	0.1122	5.2816	4.9530	4.8670	4.6370
CMD-2	γ	0.4411	0.8888	0.2874	0.1127	5.2590	4.9320	4.8460	4.6520
Rho	ϱ	0.4524	0.9188	0.2842	0.1181	5.1020	4.6000	4.5450	3.7600
Delta	δ	0.2928	0.2928	0.7207	0.0535	5.5246	5.2290	5.1541	3.8700
IC4	γ	0.4430	0.8610	0.2909	0.1110	5.3253	5.0480	4.9592	4.5250
EMD	γ	0.4434	0.8577	0.2926	0.1112	5.3680	4.9630	4.8750	4.5080
AMD	γ	0.4604	0.7587	0.3095	0.1081	5.4676	5.0590	4.9582	4.9600

* By using MW calculated on the basis of Brenet's formula $(MnO_2)_{(2n-3)}(MnOOH)_{(4-2n)}mH_2O$.
† By using MW calculated on the basis of Ruetschi's formula $Mn^{4+}_{(1-x-y)} \cdot Mn^{3+}_{y} \cdot O^{2-}_{(2-4x-y)} \cdot OH^{1-}_{(4x+y)}$.
‡ Pycnometric density in vacuum with kerosene at 40° C.

ene black (IC2) wetted with 1 ml of the electrolyte. The reference electrodes used were (Hg/HgO) in the former and the standard calomel electrode (SCE) in the latter. The cell was discharged by passing a current of 1 mA, through a zinc counter electrode. The temperature of the cell was maintained at 28° C throughout. The initial voltage of the cell (open circuit voltage, OCV) was first determined and then the cell was discharged for 5 h. The potential changes (closed circuit voltage, CCV) were manually recorded every half hour on a digital multimeter. The cell was allowed to recuperate for 16 h to determine the OCV at 5 mAh discharge. The cell discharge was continued further for 8 h per day. The cell was run until the cut off voltage of − 0.4 V against Hg/HgO and zero V against SCE was reached in the case of alkaline and acidic/neutral electrolytes respectively.

(ii) The manganese oxyhydroxide potentials. We have used the expression E (against SHE) + 0.0592 pH as this eliminates differences arising due to pH only. This was done in the light of the method suggested by Holton and co-workers [25]. The potential of the Hg/HgO electrode in 9 M KOH solution (against SHE) at 25° C has the following form:

$$E_r = E^0 - 0.0296 \log a_{H_2O} - 0.0592\,pH$$

where $E^0 = 0.926$ at 25° C, aH_2O and pH are calculated from the concentration of the electrolyte and thus, the potential of the Hg/HgO electrode (E_R) becomes 0.933 − 0.0592 pH. The manganese oxyhydroxide potential (against SHE) was obtained by adding the potential of the reference electrode (Hg/HgO) (determined by the method given above) to the potential recorded against the Hg/HgO electrode. We have, of course, chosen the experimental value of Hg/HgO as 0.936 which has been reported by Ruetschi *et al.* [26], using 34% KOH.

The models employed for comparison with the empirical data are as follows:

Model 1, Atlung and Jacobsen [1].
Model 2, Maskell, Shaw and Tye [2].
Model 3, Tye [3].
Model 4, Ruetschi [4].

3. A brief description of the models employed

As mentioned in the Introduction, Atlung [12] showed rather conclusively that even the improved relationship

$$E = E^0 + \frac{RT}{F} \ln \frac{X_{Mn^{4+}} X_{O^{2-}}}{4X_{Mn^{3+}} X_{OH^-}} \qquad (5)$$

was inadequate for the successful predictions of the observed potentials. Curves obtained on the basis of (5) showed an insufficient rate of fall of the potential. It was Tye [14] who proposed that each ion Mn^{4+}, Mn^{3+}, O^{2-}, OH^{1-} be considered as separate components of the mixture so that its activity is proportional to mole fraction. Thus

$$a_{MnO_2} = \tfrac{27}{4} X_{Mn^{4+}} X_{O^{2-}} \qquad (6)$$

$$a_{MnOOH} = 27 X_{Mn^{3+}} X_{O^{2-}} X_{OH^-} \qquad (7)$$

Atlung and Jacobsen's equation (4) is sensitive to the influence of the electronic term and from this the following equation was derived

$$E = E^0 + \frac{2RT}{F} \ln \frac{1 - r}{r} \qquad (8)$$

This agrees well for $r < 0.5$ but not for $r > 0.5$. They, therefore, modified equation (8) and it takes the following form:

$$E = E^0 + \frac{2RT}{F} \ln \frac{(1 - (1 + \alpha)r)^{(1+\alpha)}}{r(1 + \alpha r)^{\alpha}} \qquad (9)$$

Some of the basic postulates used by Maskell, Shaw and Tye [2, 3], while developing their rigorous statistical thermodynamic model for the electrochemical reduction of MnO_2 are as follows:

(i) There is a spatial independence of the proton electron pair when $(1 - r)$ moles of MnO_2 and r moles of MnOOH come together.

(ii) The oxyhydroxides formed during reduction have disordered forms of ramsdellite and groutite.

(iii) Whether the reduction takes place by proton filling or electron filling, there are two ways each in which either of these processes can occur.

The potential of such a system with respect to SHE takes the following form:

$$E_h = \frac{1}{F}(G^0_{MnO_2} - G^0_{MnOOH}) + \frac{RT}{F}\ln\frac{1-r}{r} \quad (10)$$

Equation (10) had to be modified to account for the observed potentials in the middle of the range. The modified equation is as follows:

$$E_h = \frac{1}{F}(G^0_{MnO_2} - G^0_{MnOOH}) - \frac{RT}{F} \times \ln\frac{(1-rf_m)^p(rf_m)^p(r-rf_m)^{(1-p)}r}{(1-r-rf_m)^{(1+p)}(1-r)} \quad (11)$$

where

$$p = (1-2r)/[2(1-2r+2r^2)^{1/2}]$$

and

$$f_m = \{1-[1-2r(1-r)]^{1/2}\}/2r$$

This equation, according to the authors, gave better agreement with the experimental data than equation (10) but the deviations of the theory from the experimental data in the middle region had still to be accounted for. The non-symmetrical case was, therefore, considered and the average free energy computed. The quadratic equation in f_m thus, takes the following form:

$$f_m = \{1-[1-\tfrac{8}{3}r(1-r)]^{1/2}\}/2r$$

and therefore, the expression for the potential is given as follows:

$$E_h = \frac{1}{F}(G^0_{MnO_2} - G^0_{MnOOH}) - \frac{RT}{F} \times \ln\frac{(1-rf_m)^p(rf_m)^p(r-rf_m)^{(1-p)}r}{2^p(1-r-rf_m)^{(1+p)}(1-r)} \quad (12)$$

where $p = (1-2r)/[\frac{3}{2}(1-\frac{8}{3}r^2)^{1/2}]$.

The symmetrical equation (11) was found to fit the experimental data more closely than the non-symmetrical one (12). And yet the agreement of the former with the observed potentials was not as satisfactory as it ought to have been.

Maskell *et al.* [2], therefore, carried out further refinement by taking into account two important factors:

(i) That the mixing is not ideal.

(ii) That there are two different solid solutions, one between MnO_2–$MnO_{1.75}$ and other between $MnO_{1.75}$–$MnO_{1.5}$.

In view of the above the potential is expressed differently:

$$E_h = \frac{1}{F}(G^0_{MnO_2} - G^0_{MnOOH}) - \frac{RT}{F} \times \ln\frac{(1-rf_m)^p(rf_m)^p(r-rf_m)^{(1-p)}r}{(1-r-rf_m)^{(1+p)}(1-r)} - \frac{pd}{F} \quad (13)$$

where d is the enthalpy term. If the non-symmetrical case is considered, as before, the potential takes the following form:

$$E_h = \frac{1}{F}(G^0_{MnO_2} - G^0_{MnOOH}) - \frac{RT}{F} \times \ln\frac{(1-rf_m)^p(rf_m)^p(r-rf_m)^{(1-p)}r}{2^p(1-r-rf_m)^{(1+p)}(1-r)} - \frac{pd}{F} \quad (14)$$

In the latest simplified model, Tye [3] proposes the introduction of a new parameter $r'[r' = (r-y)/(1-y)$ where y is the amount of inactive MnOOH in 1 mol of original unreduced starting material]. Incorporating this change, he proposed the following relation for the electrode potentials against SHE, which is valid over the entire homogeneous reduction range $0 < r' < 1$.

Model A

$$E = \frac{G^0_{MnO_2} - G^0_{MnOOH}}{F} + \frac{2RT}{F}\ln\left(\frac{1-r'}{r'}\right) - \frac{2.3RT}{F}\,pH \quad (15)$$

For the upper half of the reduction range, any one of the following separate equations hold good:

Model B

$$E = \frac{2(G^0_{MnO_2} - G^0_{MnOOH_{0.5}})}{F} + \frac{RT}{F} \times \ln\frac{(0.5-r')(1-r')}{4r'} - \frac{2.3RT}{F}\,pH \quad (16)$$

Model C/Model D

$$E = \frac{2(G^0_{MnO_2} - G^0_{MnOOH_{0.5}})}{F} + \frac{2RT}{F} \times \ln\frac{(0.5-r')}{r'} - \frac{2.3RT}{F}\,pH \quad (17)$$

Ruetschi's [4] model could briefly be summarized as follows. The γ/ε-MnO_2 lattice is composed of O^{2-}, OH^{1-}, Mn^{4+}, Mn^{3+} and $\boxed{Mn}$ vacancies. The structural water which is present is associated with $\boxed{Mn}$ vacancies or Mn^{3+} ions. Neither the vacancy nor the protons associated with Mn^{3+} are mobile. The protons, however, can execute jumps to adjacent O^{2-} ions under the influence of fresh protons when Mn^{4+} are being reduced to Mn^{3+}. Surface chemisorbed water is present in the form of OH^{1-} groups. The surface is presumed to consist of a 'continuous layer of Mn^{4+} vacancies'. Two surface vacancies are equivalent to one interior vacancy. Based on the above postulates Ruetschi recommended the following formula for γ/ε-MnO_2:

$$Mn^{4+}_{(1-x-y)} \cdot Mn^{3+}_{y} \cdot O^{2-}_{(2-4x-y)} \cdot OH^{1-}_{(4x+y)}$$

where x represents the fraction of Mn^{4+} ions missing in the Mn^{4+} sublattice, y is the fraction of Mn^{4+} ions replaced by Mn^{3+}. The free energy of vacancy formation determines the electrode potential difference

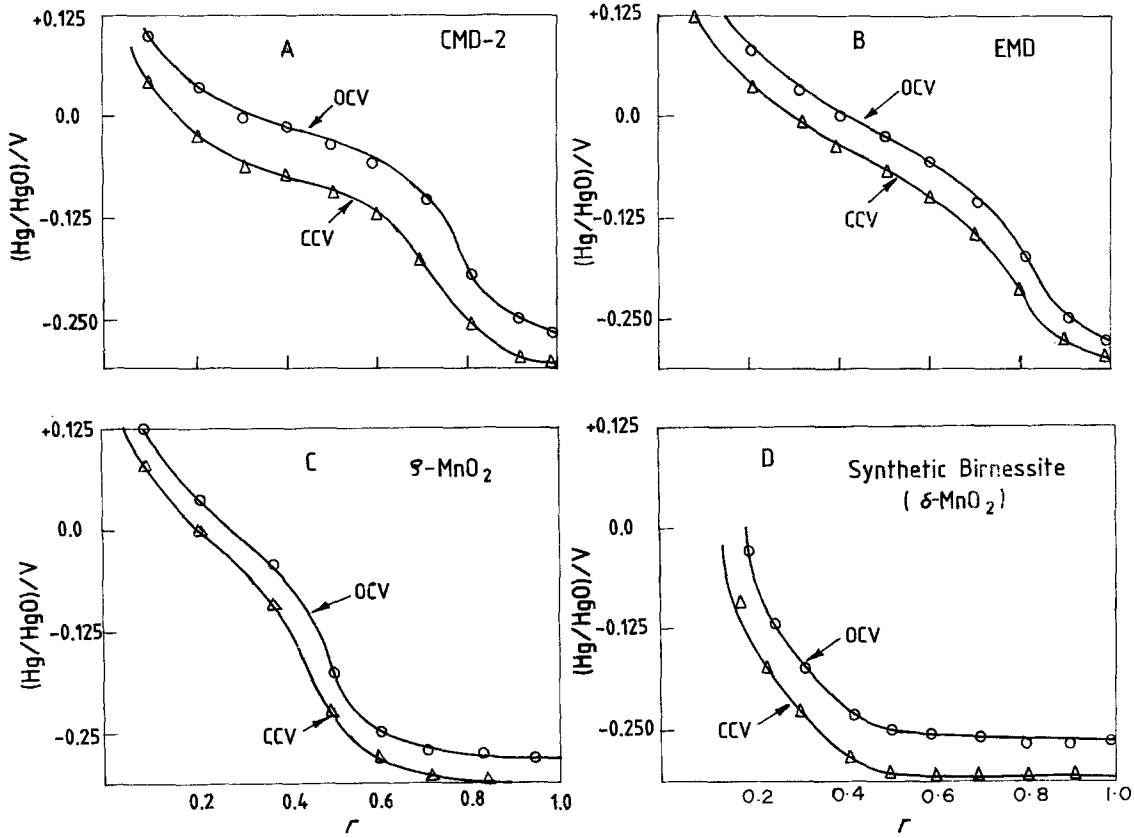

Fig. 1. Discharge curves at a constant current of 1 mA/0.1 g in 9 M KOH.

between a vacancy free oxide and cation deficient oxide. For electrochemical reduction of a single phase, the electrode potential difference is obtained by ΔG_v with respect to y. At constant y the potential is dependent on x and is given by

$$E_\gamma = E_{\gamma_0} - \frac{x}{1-x}\frac{1}{F}\frac{d(\Delta G_v)}{dy} \qquad (18)$$

for the small value of x, the electrode potential depends linearly on x and consequently on water content. Equation (18) is, therefore, expressed as

$$E_\gamma = E_{\gamma_0} - \frac{\%H_2O}{44}\frac{1}{F}\frac{d(\Delta G_v)}{dy} \qquad (19)$$

Applying the method of statistical thermodynamics and limiting the discussion to the configurational partition function, the cation vacancy model leads to the following situation. At a fixed vacancy fraction x, there are in total $(1-x)Mn^{4+}$ sites available for the distribution of yMn^{3+} ions. For each configuration, y protons can be distributed independently into $(2-4x)O^{2-}$ sites if all O^{2-} sites are equally available. On the other hand they can distribute themselves into $(1-px+y)O^{2-}$ sites if only pyramidally coordinated sites are available during reduction. Neglecting interaction terms, the electrode potential expressions were given as follows:

For equally available sites:

$$E_\gamma = E'_{\gamma_0} + \frac{RT}{F}\ln\frac{1-x-y}{y} + \frac{RT}{F}\ln\frac{2-4x-y}{y} \qquad (20)$$

and for only pyramidal available sites:

$$E_\gamma = E''_{\gamma_0} + \frac{RT}{F}\ln\frac{1-x-y}{y} + \frac{RT}{F}\ln\frac{1-px-y}{y} \qquad (21)$$

4. Results and discussion

It will be observed from Figs. 1–3 that in almost all the cases the potential remains more or less constant from $r \simeq 0.8$ to $r \simeq 1$ in alkaline electrolyte. Holton, Maskell and Tye [25] reported recently a constant potential after $MnO_{1.62}$ corresponding to $r \simeq 0.8$ to $r \simeq 1$. This constant potential range is attributed, by them, to the formation of Mn_3O_4 from γ-MnOOH. The horizontal potential range observed in the case of γ-MnO_2 samples of ours, however, is not as pronounced as the one obtained by them [25]. The ϱ- and δ- MnO_2, clearly indicate a much larger range of this horizontal potential. The hypothesis of Tye and co-workers, therefore, seems to be tenable especially in the light of partial conversion of γ-MnO_2 to δ-MnO_2 which in turn is converted to Mn_3O_4 through γ-MnOOH. Whereas they have studied the potentials of the various oxyhydroxides by reducing MnO_2 chemically [25], this particular study involves galvanostatic reduction. The deviation of the horizontal potential observed here from the one which is observed by Holton *et al.* [25], does not seem to be very significant. The dramatic, or abrupt, fall of potential from $MnO_{1.7}$ to $MnO_{1.63}$ corresponding to $r \simeq 0.63$ to $r \simeq 0.78$ is also seen in the case of our γ-MnO_2

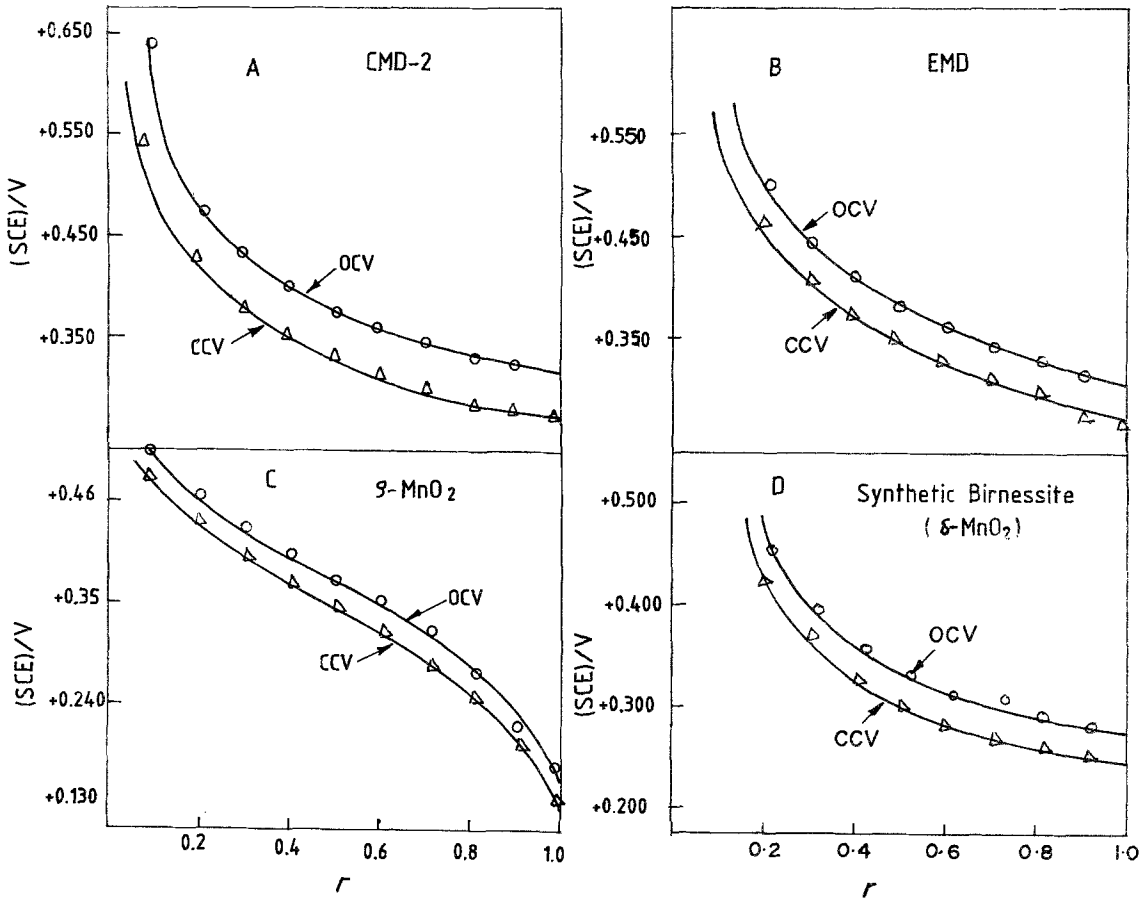

Fig. 2. Discharge curves at a constant current of 1 mA/0.1 g in 5 M NH_4Cl + 2 M $ZnCl_2$.

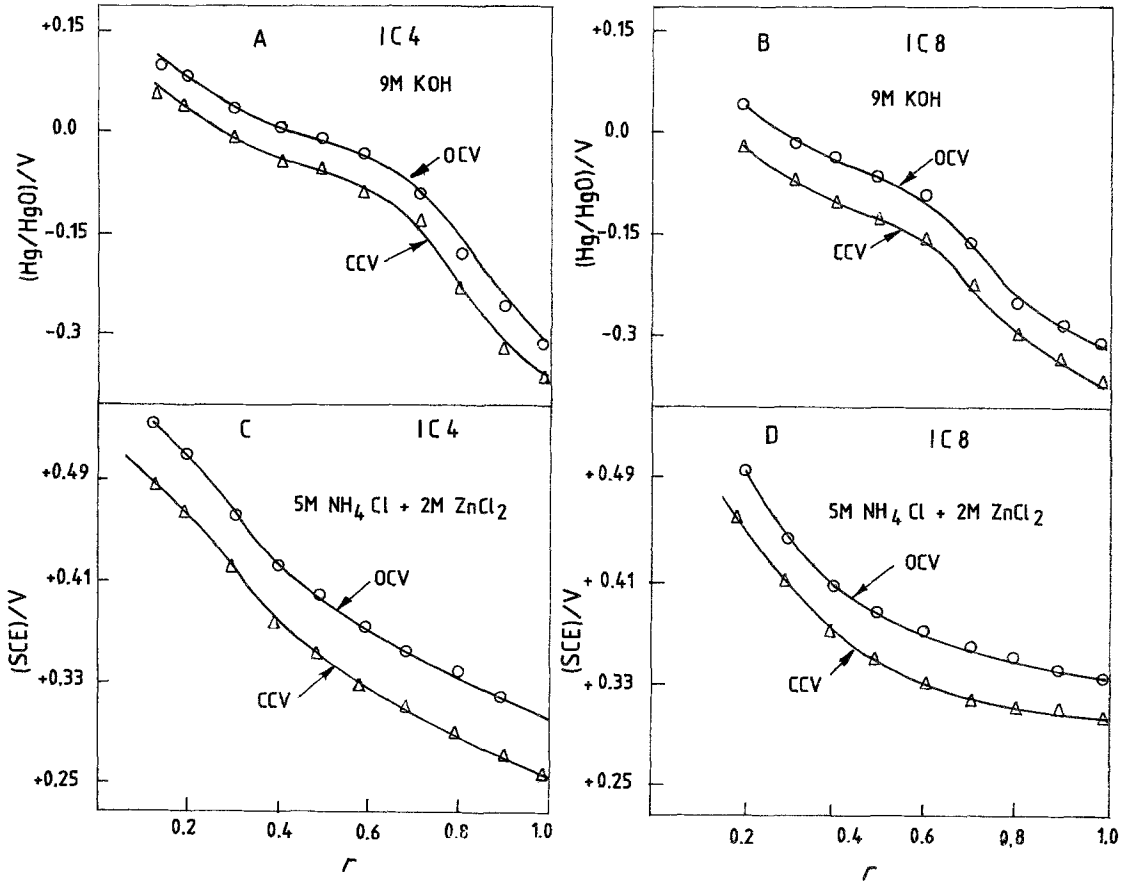

Fig. 3. Discharge curves at a constant current of 1 mA/0.1 g.

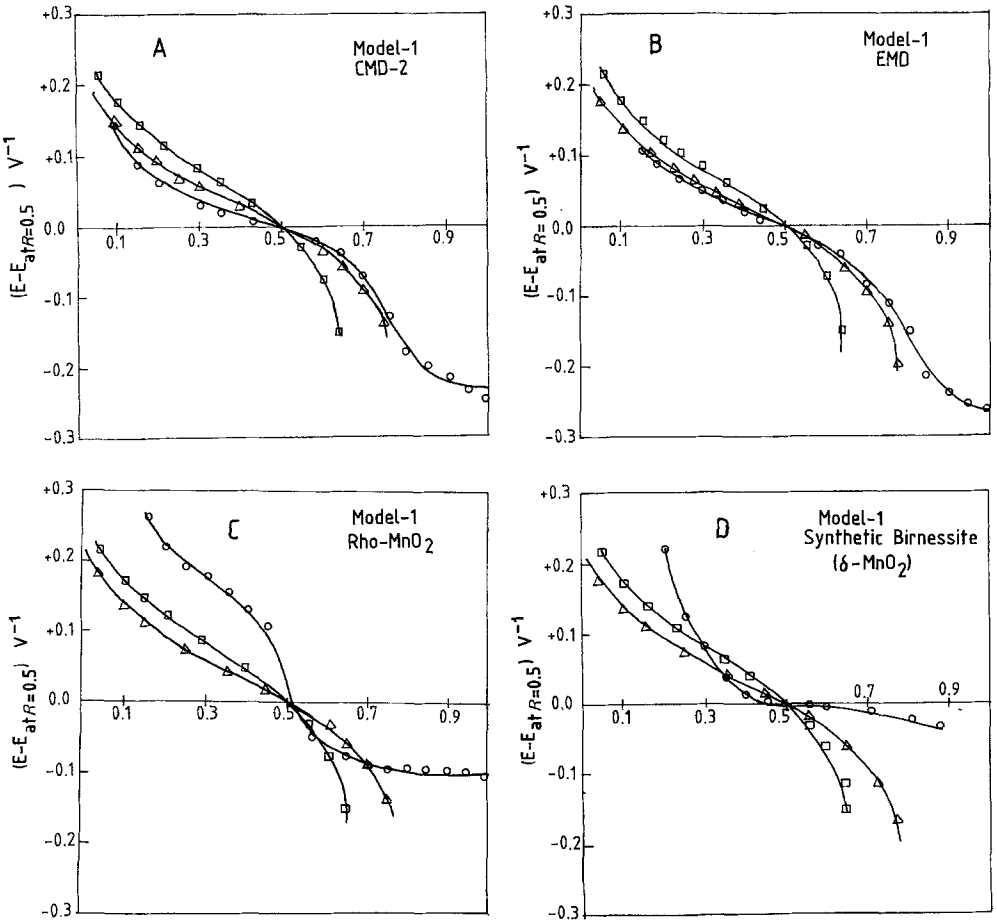

Fig. 4. Calculated and experimental curves of: (A) CMD-2; (B) EMD; (C) ϱ-MnO_2; (D) synthetic birnessite (δ-MnO_2); (○) experimental, (△) calculated ($\alpha = 0.25$); (□) calculated ($\alpha = 0.47$) both from equation (9).

samples but the fall is of a slightly lower order, i.e. approximately 180 mV. This is not surprising if it is kept in mind that the potentials observed were under forced reduction (galvanostatic reduction). (The addition of graphite or acetylene black could have some influence on the discharge curve as well.)

The applicability of Model 1 was reported earlier [27]. It was, however, felt that Model 1 ought to be tested more extensively and the results juxtaposed with those obtained with the other Models for comparison.

The potentials of the oxyhydroxide system as a function of reduction parameter r of the MnO_2 samples presented in this work were calculated with the help of equation (9). CMD-2 gave an excellent agreement with Model 1 up to $r \simeq 0.8$ with $\alpha = 0.25$ (Fig. 4A). On the other hand an earlier attempt of ours to apply this model with $\alpha = 0.25$ for both IC8 and CMD-2 was not very satisfactory. In fact it was with $\alpha = 0.47$ that the observed potential curves had given a much better fit. The preparation of CMD-2 was similar to A_5, of our earlier publication [17]. However, the procedure was slightly modified to get a material of higher density. The addition of $NaClO_3$ was done slowly over a period of time (1 h). This procedure seems to have changed it slightly in terms either of less disorder in the structure or in the intergrown α or β domains (021 line happens to be the 100 intensity line in this case as against 221 line in the case of erstwhile A_5 sample). It appears, therefore, that homogeneous phase reduction range does change slightly even with a slight change in the method of preparation or with miniscule changes in cell-design and/current density. The observed potential curve of IC8 also matches with the theoretical values computed with $\alpha = 0.25$ (not shown). In short, all the cases of MnO_2 considered here seem to yield a reasonable agreement with Model 1 until $r \simeq 0.8$ and deviate, either marginally or substantially, only from this point onwards.

The EMD prepared by the method identical to the one adopted for IC4 also gave a good agreement with the theory (Fig. 4B).

The δ-MnO_2 according to Giovanoli [28] is not a true MnO_2 modification but a cognate member of the manganate family; the true name being synthetic birnessite. The most marked deviation from the theoretical value is observed in this case. This further vindicates the proposition of Giovanoli that the structure of δ-MnO_2 is altogether different from the γ-MnO_2 family. Further, it will be seen that none of the models discussed here (Figs. 4D, 6C) seems to fit the observed discharge behaviour of this particular variety. The failure of δ-MnO_2 to fit any one of the theoretical models should not be surprising. A comparison of Figs. 4C, 4D reveals the substantial deviation from the theory. But the type of deviation observed in the case of ϱ-MnO_2 is of degree and not of kind, whereas the deviation shown by δ-MnO_2 seems to be both of kind and degree.

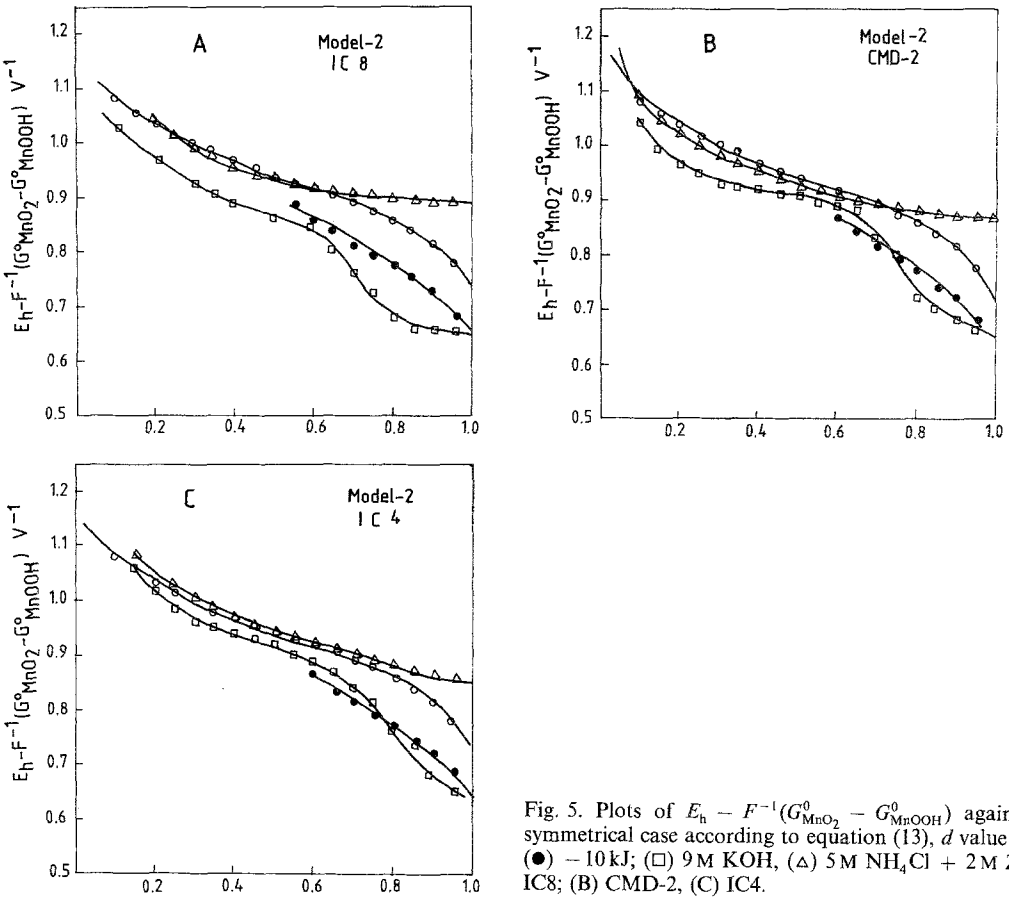

Fig. 5. Plots of $E_h - F^{-1}(G^0_{MnO_2} - G^0_{MnOOH})$ against r for the symmetrical case according to equation (13), d value (○) ∓ 2.5 kJ, (●) -10 kJ; (□) 9 M KOH, (△) 5 M NH_4Cl + 2 M $ZnCl_2$ of: (A) IC8; (B) CMD-2, (C) IC4.

4.1. *Maskell, Shaw and Tye Model 2 equation (13)*

4.1.1. Alkaline electrolyte. As indicated in an earlier section the potentials of the oxyhydroxide system in the case of CMD-2 in alkaline medium were calculated using equation (13) and compared with the experimental values (see Fig. 5B). There seems to be a considerable difference between the calculated and the observed potentials (OCV). Further, even the profile shows a pronounced deviation, specially in the lower half, i.e. $0.5 < r < 1$. This certainly cannot be attributed to an experimenal error as this behaviour has also been reported by other workers [29]. Fig. 5A and 5B clearly reveal the divergence of the experimental data from the Model 2 values in the lower half in the case of IC8 and CMD-2. If -10 kJ is assumed to be the enthalpy change due to the mixing of type A and type B protons, then the theoretical curve in the lower half falls below, in fact approximately by about 70–80 mV, and this corresponds better with the observed potential. This is the case with electrolytic MnO_2 (also see Fig. 6A).

The ϱ and δ-MnO_2 do not fit in any case as is amply evident from the OCV curves (see Fig. 1) themselves. The closer correlation with the experimental curves when -10 kJ is chosen for the lower half only implies a drop in f with increase in r values. This means that either a substantial number of protons must be switching from type B to type A and not merely a few moles, assuming that the proton filling mechanism holds or some other processes leading to enthalpy change take place. It is rather surprising that a more negative d-value is required to be used to get a better fit in the lower half. So, prima facie, it seems to be the electronic delocalization mechanism and not hydrogen bonding that operates in the $MnO_{1.75}$–$MnO_{1.5}$ range. Holten and co-workers [25] reported the emergence of γ-MnOOH as a separate phase at about $MnO_{1.63}$. This, we feel, could be one of the reasons for the deviation of the observed OCV curve in alkaline medium.

Experimental data on the discharge products (communicated to the Journal of Power Sources) and the OCV curves reported here indicate that the homogeneous phase of the one-electron reaction ends at about $MnO_{1.6}$ i.e. $r \simeq 0.8$ and from this point onwards up to $r \simeq 1$ the OCV takes a horizontal form clearly indicating a beginning of the heterogenous reaction from $MnO_{1.7}$ onwards. If we assume this to be the case then any mechanism that attempts to predict the behaviour of the potential in the lower half should take this factor into account. At this stage of the argument, we do not know whether the improved agreement of the observed potential with the theory (when -10 kJ is chosen) is fortuitous or not.

4.1.2. In 5 M NH_4Cl + 2 M $ZnCl_2$ electrolyte. Model 2 seems to fit the experimental data in acidic/neutral medium far better than the one in the alkaline medium in case of both CMD and EMD (see Figs. 5B, 6A).

Fig. 5B clearly reveals a far better correspondence with theoretical values right up to $r \simeq 0.9$. This theoretical curve (Fig. 5B) was drawn with an enthalpy mixing factor of -2.5 kJ and $+2.5$ kJ on either side of

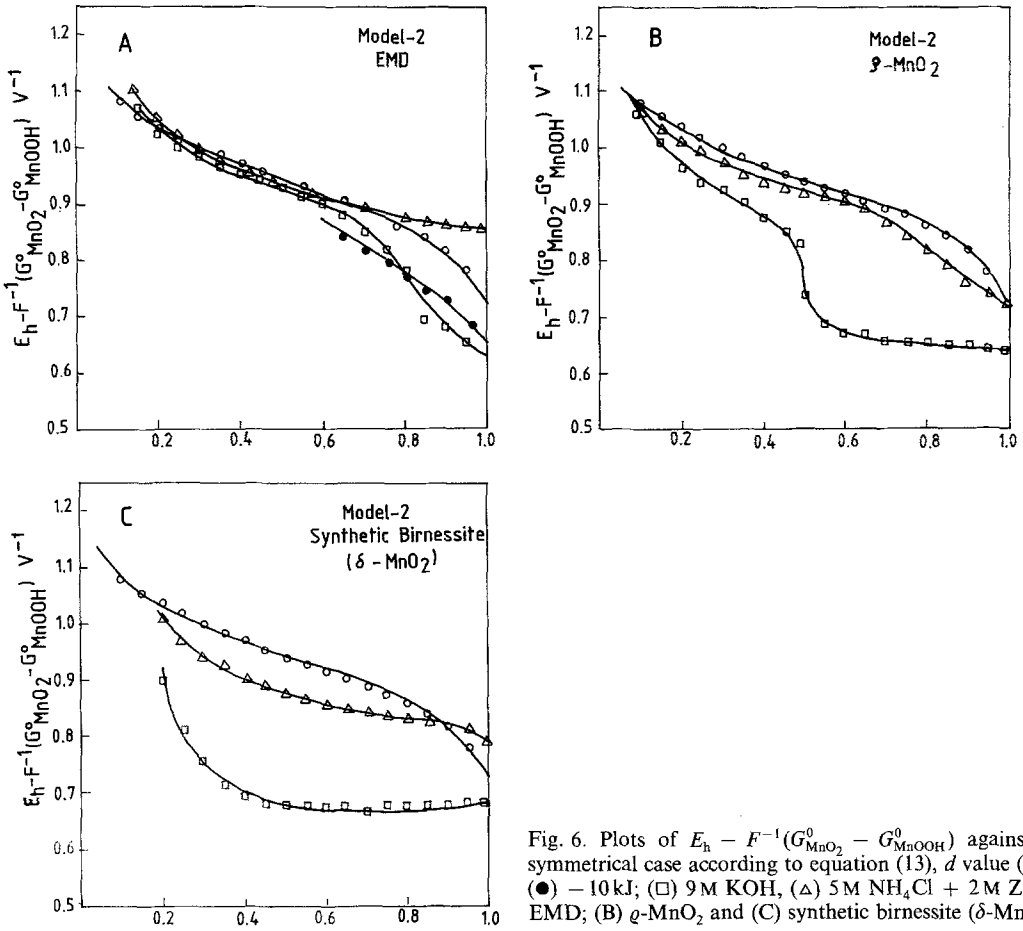

Fig. 6. Plots of $E_h - F^{-1}(G^0_{MnO_2} - G^0_{MnOOH})$ against r for the symmetrical case according to equation (13), d value (○) ∓ 2.5 kJ, (●) -10 kJ; (□) 9 M KOH, (△) 5 M NH_4Cl + 2 M $ZnCl_2$ of: (A) EMD; (B) ϱ-MnO_2 and (C) synthetic birnessite (δ-MnO_2).

the mid-reduction point. The reasonably successful application of the model of Maskell and co-workers [2] to both CMD and EMD in neutral/acidic electrolyte seems to suggest that structural variations, if any, between γ-CMD and γ-EMD (EMD is reported to have an ε-MnO_2 structure i.e. NiAs type) [30] do not play any significant role. Also the incorporation of non-ideal mixing and consequently the inclusion of the enthalpy factor (ΔH) seems to be almost inevitable if we are to get a realistic experimental match with the theoretical values. The failure of equations (11) and (12) to account for the observed potential-reduction curve satisfactorily becomes obvious. Further, the importance of the enthalpy mixing term becomes all the more obvious in Ruetschi's model (Fig. 8) as the calculated potentials deviate from the observed ones by about 20–30 mV.

One curious thing that has emerged is this. In the plot of OCV against r, in the case, not only of CMD, but also other polymorphic modifications, the curve does not have a classical S-shape. In fact the potentials remain constant from about +0.35 V (against SCE) onwards. It appears, therefore, that the observed homogeneous reduction range ends a little earlier at about $r = 0.5$ and nor $r = 1$. This has also been observed by Kozawa [31]. Maskell *et al.* [15] have reproduced some of the experimental curves of Huber and Bauer [32] and Neumann and Roda [9] of potential against r which are distinctly different from the ones which are obtained in this work, but the experimental conditions were quite different. On the other hand, all OCV against r curves are very similar to the ones reported by Kozawa [31]. The longer range of constant potential observed in case of acidic/neutral electrolyte, in all samples except ϱ-MnO_2 indicates the formation of some new phases or even heterolyte as the potentials remain constant even beyond $r = 1$, i.e. $MnO_{1.5}$.

The OCV curve of ϱ-MnO_2 in acidic/neutral electrolyte is a classical S-shaped curve. It is probably because of this that both Model 2 (Fig. 6B) and Model 4 (Fig. 10) yield a much better agreement with the observed potentials in this case. This is all the more surprising in view of the fact that ϱ-MnO_2 is a poorly crystallized γ-MnO_2. The deviation of the observed curve from $r = 0.5$ onwards is, therefore, understandable. In case of both IC4 and EMD, the experimental fit with the theory is almost perfect up to $r \simeq 0.85$. The subsequent deviation is also marginal (Fig. 5C, 6A). On the other hand in the case of IC8 and CMD-2 the deviation from the theoretical curve begins around $r = 0.7$ and is a little more pronounced. This has also been reported by Maskell *et al.* [2]. This deviation is attributed by them to the formation of γ-MnOOH at that stage of the reduction. δ-MnO_2 discharge behaviour is a case by itself. The observed potential profile is markedly different from the theoretical one (see Fig. 6C).

4.2. *Tye Model 3 (15, 16)*

The latest model of Tye [3], which we have touched

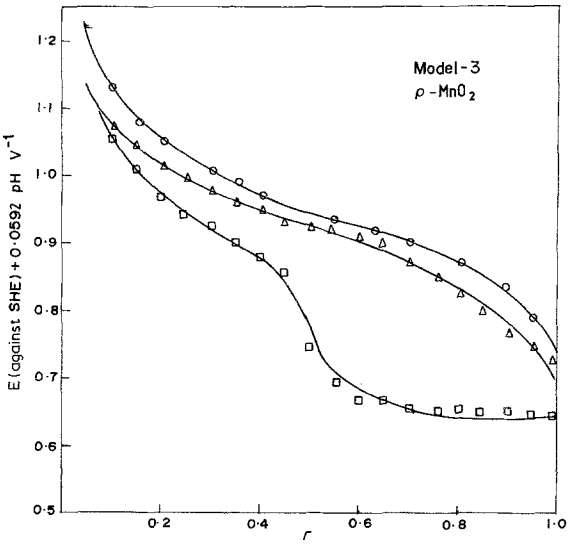

Fig. 7. Plots of E (against SHE) + 0.0592pH against r according to equations (15, 16) (○) of Rho; (□) 9M KOH and (△) 5M NH_4Cl + 2M $ZnCl_2$.

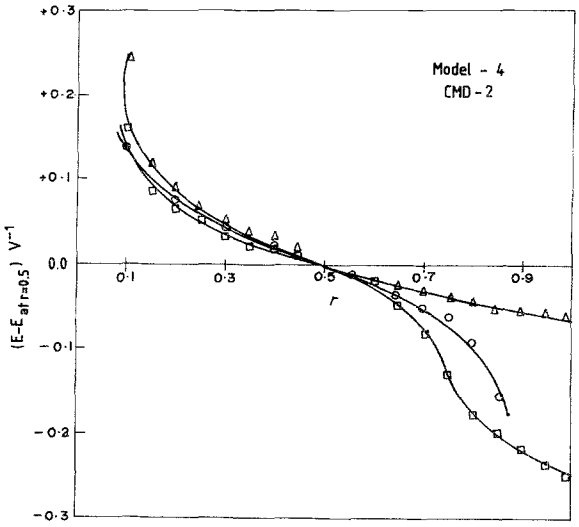

Fig. 8. Variation of electrode potential with r according to equation (21) for $p = 2$ (○) of CMD-2; (□) 9M KOH and (△) 5M NH_4Cl + 2M $ZnCl_2$.

upon in section 3, identifies the end members of the two solid solutions as $MnOOH_{0.5}$ and MnOOH, MnO_2 being the starting member in both cases. Earlier it was thought that the solid solution ranges are as follows:

(i) MnO_2 – $MnOOH_{0.5}$
(ii) $MnOOH_{0.5}$ – MnOOH

If the latter is taken to be the case then the double S-shaped curve results. This is not the case in reality. Hence the postulated change in the composition.

Our results in acid/neutral electrolyte indicate that there is no perceptible difference in the theoretical values derived from Model 2 or Model 3. We do not observe any significant improvement in the experimental match with Model 3. The internal differences, however, in the values calculated from Model 2 and Model 3 are not insignificant. But the fact remains that satisfactory correlation with the observed potentials is still elusive. Both the models seem to hold equally well in the first half and both deviate, significantly or marginally from $r \simeq 0.85$ onwards. It is only in the case of ϱ-MnO_2 that Model 3 yields a better agreement than Model 2 in acidic medium (Fig. 7). The observed curves in the alkaline medium, also, therefore, deviate to the same extent as they do in the case of Model 2.

4.3. *Ruetschi Model 4*

This model, which is a bit larger in scope, attempts to predict the electrode potentials based on Mn vacancies. The inherent limitation of this model is that it predicts the values only up to $r = 0.8$ as against others which go right up to $r = 1$. On the other hand, however, this model gives a good account of itself in predicting and correlating some of the crucial physical properties such as structural/combined water, pycnometric density, electronic conductivity, proton transfer rate and electrochemical activity with $\boxed{\text{Mn}}$ vacancies. In fact the experimental fit of some of the observed values of these properties with those predicted by Ruetschi is exceptionally good. This is the case with almost all γ-MnO_2 samples i.e. IC4, IC8 as well as EMD, CMD, AMD, ϱ-MnO_2 and δ-MnO_2 prepared by us (Table 3).

The linear relationship between the structural water and vacancy fraction, x, is shown in Fig. 11 (both with $y = 0$ and $y = 0.1$ where y is the fraction of Mn^{4+} ion replaced by Mn^{3+} ion). In a way y could be considered as an equivalent of r_0, i.e. initial MnOOH present in virgin MnO_2. It will be seen from Fig. 11 that even the earlier samples from this laboratory [17] (Table 4)

Table 3. Correlation of physical and electrochemical properties of the manganese dioxides prepared in this work

Sample	*m*	*x*	*y*	*MW* (g)	% H_2O		% C_w	% C_v	*V* $(nm)^3$	*Density* g cm^{-3}		*Pycnometric density* g cm^{-3}
					$y = 0$	$y = 0.1$				$y = 0$	$y > 0$	
IC8	0.0806	0.03872	0.0741	84.97	1.642	2.702	98.44	102.45	0.1109	5.089	4.999	4.667
CMD-1	0.1384	0.06472	0.0408	83.65	2.788	3.864	97.29	98.59	0.1122	4.953	4.867	4.637
CMD-2	0.1374	0.06428	0.0398	83.67	2.768	3.845	97.31	98.21	0.1127	4.932	4.846	4.652
Rho	0.2077	0.09405	0.0280	82.15	4.125	5.221	95.95	90.25	0.1187	4.600	4.545	3.760
Delta	0.1124	0.05320	0.0788	84.23	2.275	3.345	97.80	–	0.0535	5.229	5.145	3.870
IC4	0.1095	0.05191	0.0600	84.30	2.218	3.217	97.85	101.06	0.1110	5.048	4.959	4.525
EMD	0.1624	0.07510	0.0583	83.11	3.255	4.339	96.82	98.33	0.1112	4.963	4.875	4.507
AMD	0.1096	0.05195	0.0612	84.29	2.220	3.289	97.86	101.03	0.1081	5.059	4.958	4.960

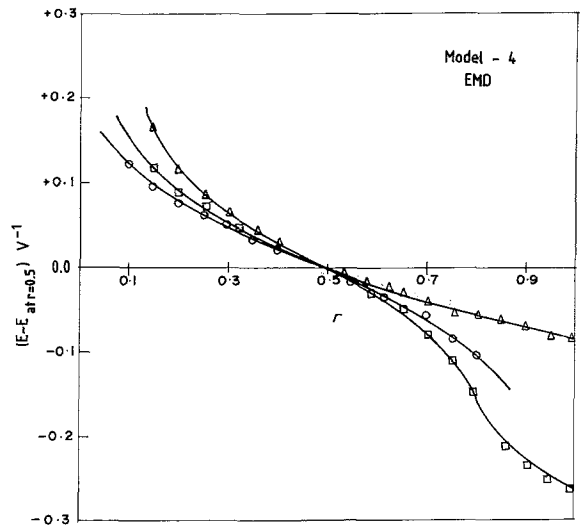

Fig. 9. Variation of electrode potential with r according to equation (21) for $p = 2$ (○) of EMD; (□) 9 M KOH and (△) 5 M NH_4Cl + 2 M $ZnCl_2$.

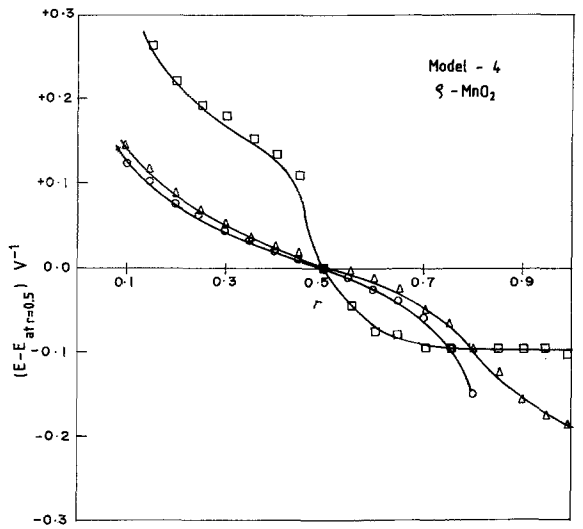

Fig. 10. Variation of electrode potential with r according to equation (21) for $p = 2$ (○) of Rho; (□) 9 M KOH and (△) 5 M NH_4Cl + 2 M $ZnCl_2$.

follow the relationship remarkably well. The relationship between theoretical electrochemical capacity C_w (maximum) and the vacancy fraction x proposed by Ruetschi is as follows:

$$C_w = \frac{(1 - x - y)26.80}{MW} \text{ (Ah g}^{-1}\text{)}$$

where 26.80 is the theoretical mAh and MW is computed from the following formula:

$$Mn^{4+}_{(1-x-y)} Mn^{3+}_{y} O^{2-}_{(2-4x-y)} OH^{1-}_{(4x+y)}$$

Our results agree well with the values predicted by this model (Fig. 12). Then again the relationship between the relative proton transfer rate against vacancy fraction x is shown in Fig. 13. Proton transfer rate P_t is defined as

$$P_t = \nu[OH^{1-}][O^{2-}]$$

where ν is a jump frequency.

It is obvious from the Figs. 8, 9, 10 that Ruetschi's model is rather inadequate for successful prediction of observed potentials of the samples investigated here. The only exception is ϱ-MnO_2. It is rather significant that the discharge curve of this sample in acidic/neutral electrolyte seems to fit this model reasonably well. The profiles of the observed potentials in the case of both neutral/acidic as well as alkaline electrolyte deviate substantially in the lower half and in some cases (Figs. 8, 9, 10) in the upper half as well. It is, therefore, felt that the enthalpy mixing factor which was taken into account by Tye in Model 2 has to be incorporated in this model. The model thus refined might conform to the experimental data with a greater degree of exactitude than obtained so far.

The simpler equations presented in the refined model [3] of Tye are also not satisfactory in view of the lack of experimental match with the theoretical values. In fact, even the profiles of the observed potentials are different.

5. Summary

The potentials of the oxyhydroxides varying from

Table 4. Correlation of physical and electrochemical properties of some earlier samples [17]

Sample	*m*	*x*	*y*	*MW* (g)	% H_2O		% C_w	% C_v	*V* $(nm)^3$	*Density* $g cm^{-3}$	
					$y = 0$	$y = 0.1$				$y = 0$	$y > 0$
A_2	0.11	0.052	0.0285	84.29	2.23	3.29	97.86	98.41	0.1139	4.914	4.83
A_3	0.15	0.0698	0.0287	83.38	3.015	4.095	97.08	96.47	0.1139	4.861	4.778
A_4	0.24	0.1071	0.0371	81.48	4.736	5.84	95.35	96.63	0.1093	4.952	4.864
A_5	0.21	0.095	0.019	82.10	4.17	5.266	95.00	93.96	0.1142	4.754	4.695
B_1	0.16	0.074	0.035	83.17	3.20	4.289	96.88	94.63	0.1158	4.773	4.689
B_2	0.213	0.096	0.026	82.05	4.21	5.313	95.86	94.36	0.1133	4.811	4.727
D_1	0.301	0.130	0.765	80.32	5.831	6.950	94.25	80.56	0.1165	4.581	4.474
D_2	0.245	0.109	0.0793	81.38	4.825	5.942	95.25	84.55	0.1135	4.763	4.655
D_3	0.262	0.116	0.0670	81.05	5.14	6.25	94.95	84.57	0.1152	4.675	4.595
D_4	0.547	0.215	0.0447	75.99	10.19	11.28	89.88	73.52	0.1191	4.240	4.122
D_5	0.4284	0.1764	0.0494	77.96	8.153	9.30	86.41	79.19	0.1156	4.479	4.403
D_6	0.145	0.067	0.056	83.50	2.917	4.00	97.16	93.04	0.1181	4.679	4.601

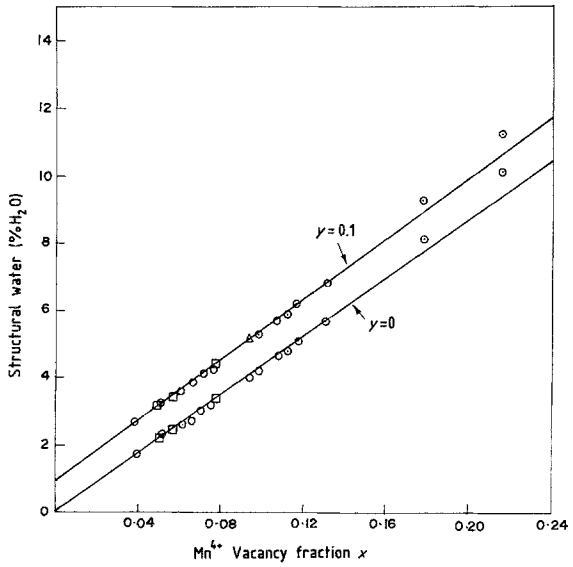

Fig. 11. Structural water content (%) as a function of Mn^{4+} vacancy fraction x. (○) CMD; (□) EMD; (⊙) AMD.

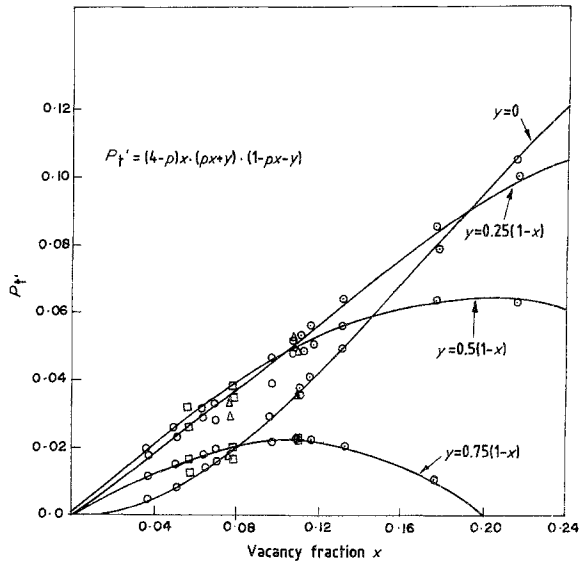

Fig. 13. Relative proton transfer rate as a function of Mn^{4+} vacancy fraction x. (○) CMD, (□) EMD, (⊙) AMD.

$r = r_0$ to $r = 1$ were calculated by using equations (9), (13), (14), (15), (16), (20) and (21) in both acidic/neutral and alkaline electrolytes. These calculated potentials were plotted against r the reduction parameter. The observed potentials of all the samples prepared in this work were also plotted similarly and juxtaposed with the calculated ones in order to discover which model yields the best agreement. It has been found that Model 2, represented by equation (13), yielded, by far, the best fit with the experimental data in acidic/neutral electrolyte, though not in alkaline medium. The agreement between calculated and observed potentials in the alkaline medium is, however, improved if an appropriate value of the parameter d (enthalpy of mixing) is chosen. It has been found that if d is chosen to be -10 kJ in the lower half of the reduction range then the experimental fit with the calculated potentials of CMD-2, IC4, EMD shows some improvement. Simplified Model 3 does not seem to yield any significant improvement in the calculated potentials. The model proposed by Ruetschi needs further refinement for its successful application to the discharge behaviour of γ/ε-MnO_2. The case of δ-MnO_2 seems to belong to a different category altogether.

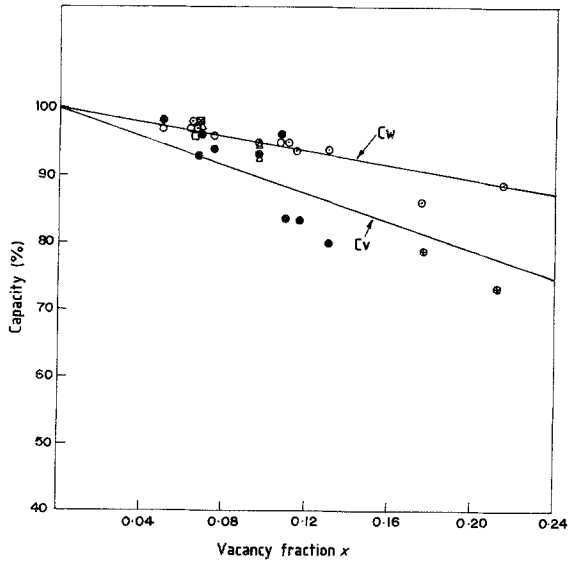

Fig. 12. Theoretical electrochemical capacity per unit weight, C_w and per unit volune C_v as a function of Mn^{4+} vacancy fraction for $y = 0$. C_w (○) CMD, (□) EMD, (⊙) AMD; C_v (●) CMD, (⊠) EMD, (⊕) AMD.

Acknowledgement

We are grateful to Professor F. L. Tye, Middlesex Polytechnic, London and to Professor Paul Ruetschi of Leclanche Switzerland. We also thank Professor V. R. Pai Vernekar, I.I.Sc., Bangalore, Dr B. K. Basu, T.I.F.R., Bombay, Late Dr H. N. Siddiquie, Director, Mr B. G. Wagle, Mr N. H. Hashimi and Mr R. R. Nair, N.I.O., Dona Paula, Goa.

References

[1] S. Atlung and T. Jacobsen, *Electrochim. Acta* **26** (1981) 1447–1456.
[2] W. C. Maskell, J. E. A. Shaw and F. L. Tye, *ibid.* **28** (1983) 225–230; 231–235.
[3] F. L. Tye, *ibid.* **30** (1985) 17–23
[4] P. Ruetschi, *J. Electrochem. Soc.* **131** (1984) 2737–2744.
[5] J. J. Coleman, *Trans. Electrochem. Soc.* **90** (1946) 545.
[6] R. S. Johnson and W. C. Vosburgh, *J. Electrochem. Soc.* **100** (1953) 471.
[7] A. B. Scott, *ibid.* **107** (1960) 941.
[8] F. Kornfeil, *ibid.* **109** (1962) 349.
[9] K. Neumann and E. V. Roda, *Z. Elektrochem. Ber. Bunsenges. Phys. Chem.* **69** (1965) 347.
[10] A. Kozawa and R. A. Powers, *J. Electrochem. Soc.* **113** (1966) 870.
[11] *Idem., Electrochem. Technol.* **5** (1967) 535.
[12] S. Atlung, Paper presented at the I.S.E. Meeting, Div. 6, Kelkheim, 1973.
[13] *Idem.*, 'MnO_2 Symp. Proc. Cleveland. OH.', (edited by A. Kozawa and R. R. Brood) **1** (1975) 47.
[14] F. L. Tye, *Electrochim. Acta* **21** (1976) 415.
[15] W. C. Maskell, J. E. A. Shaw and F. L. Tye, *J. Power Sources* **8** (1982) 113.
[16] *Idem., J. Appl. Electrochem.* **12** (1982) 101.
[17] J. B. Fernandes, B. D. Desai and V. N. Kamat Dalal, *Electrochim. Acta* **28** (1983) 309–315.
[18] R. M. McKenzie, *Aust. J. Soil. Res.* **8** (1970) 97.

[19] R. Giovanoli, E. Stähli and W. Feitknecht, *Helv. Chim. Acta* **53** (1970) 453.
[20] K. Takahashi, 'Electrochemistry of Manganose Dioxide and Manganese Dioxide Batteries in Japan', Vol. 1 & 2 (Vol. 2) (edited by S. Yoshizawa, K. Takahashi and A. Kozawa) (1971) p. 34.
[21] D. M. Holten and F. L. Tye, MnO_2 Symp. Proc. Tokyo. Jpn., Vol. 2 (edited by B. Schumm, Jr., H. M. Joseph and A. Kozawa) (1980) 244.
[22] T. Matsumura, *ibid.* (1980) 596.
[23] B. D. Desai, R. A. S. Dhume and V. N. Kamat Dahl, *J. Power Sources*. (in press).
[24] J. B. Fernandes, B. D. Desai and V. N. Kamat Dalal, *Electrochim. Acta* **29** (1984) 181.
[25] D. M. Holten, W. C. Maskell and F. L. Tye, Presented at 14th International Power Sources Symposium held at Brighton, (17–20 Sept., 1984) 1–25 (Pre-publication Text).
[26] Cited in Alkaline Storage Batteries, (edited by S. U. Falk and A. J. Salkind) John Wiley and Sons, Inc. (1969) 535.
[27] J. B. Fernandes, B. D. Desai and V. N. Kamat Dalal, *J. Appl. Electrochem.* **15** (1985) 358.
[28] R. Giovanoli, *Chimia* **23** (1969) 472.
[29] A. Kozawa, Proceedings of the 11th International Symposium 1978. 'Power Sources 7' (edited by J. Thomson) Academic Press, London (1979) p. 485.
[30] P. M. de Wolff, J. W. Visser, R. Giovanoli and R. Brutsch, *Chimia* **32** (1978) 257.
[31] A. Kozawa, 'Manganese Dioxide Batteries' Vol. I (edited by K. V. Kordesch), Marcel Dekker (1972) 429.
[32] R. Huber and J. Bauer, *Electrochem. Technol.* **5** (1967) 542.